

Modelling the linear viscoelastic behavior of silicate glasses near the glass transition point

Aleksey D. Drozdov and Jesper deC. Christiansen

Department of Production

Aalborg University

Fibigerstraede 16, DK-9220 Aalborg, Denmark

Abstract

A model is derived for the viscoelastic response of glasses at isothermal uniaxial deformation with small strains. A glass is treated as an ensemble of relaxing units with various activation energies for rearrangement. With reference to the energy-landscape concept, the rearrangement process is thought of as a series of hops of relaxing units (trapped in their potential wells on the energy landscape) to higher energy levels. Stress-strain relations are developed by using the laws of thermodynamics. Adjustable parameters are found by fitting experimental data in torsional dynamic tests on a multicomponent silicate glass at several temperatures near the glass transition point.

Key-words: Silicate glasses, Dynamic tests, Viscoelasticity, Glass transition

1 Introduction

This study is concerned with the viscoelastic behavior of silicate glasses at uniaxial deformation with small strains. This subject has been a focus of attention in the past decade because of numerous applications of vitreous silica in industry (that range from waveguides and optical fibers to semiconductor wafers and tire additives [1]) and the key role of multicomponent silicate glasses in geological processes [2].

Observations in static and dynamic mechanical tests on silicate glasses are conventionally fitted by using such phenomenological approaches as (i) the generalized Maxwell model [3], (ii) the KWW (Kohlrausch-Williams-Watt) formula [4], and (iii) linear stress-strain relations with fractional derivatives [5]. The objective of this paper is to develop constitutive equations for the linear viscoelastic response of an amorphous glass based on a micro-mechanical concept and to validate these relations by matching experimental data in torsional oscillatory tests on a multicomponent silicate glass.

2 A micro-mechanical model

A silicate glass is thought of as an ensemble of cooperatively rearranging regions (CRRs), where mechanical stress relaxes due to rotational rearrangement of small clusters of atoms (consisting of a few SiO_4 tetrahedra) that change their configuration as they are agitated by thermal fluctuations.

To describe the viscoelastic response of a glass in dynamic tests with a restricted window of frequencies, we distinguish two types of relaxing units: (i) active CRRs that can rearrange during the experimental time-scale, and (ii) passive CRRs whose characteristic time for rearrangement substantially exceeds the duration of a test. An active CRR is entirely characterized by the energy, v , of the thermal fluctuations necessary for rearrangement. With reference to the energy-landscape concept [6], an active CRR is modelled as a material point trapped in a potential well on the energy hypersurface in the phase space. The well is characterized by its depth, v , with respect to some reference (liquid-like) energy level. The point spends most time being located at the bottom level of its potential well. At random instants, the point hops to higher energy levels as it is thermally agitated. If the point does not reach the liquid-like energy level in a hop, it returns to the bottom level of its well being unaltered. When the point reaches the reference level in a hop, the CRR changes its configuration and accepts the current state of a deformed medium as its reference state.

The kinetics of rearrangement is uniquely determined by the temperature-dependent attempt rate ν_0 (the number of hops in a well per unit time) and the distribution function, $q(u)$, for hops with various heights ($q(u)du$ is the probability of a hop whose height belongs to the interval $[u; u + du]$). We adopt the exponential distribution of intensities of hops [7],

$$q(u) = \frac{1}{V} \exp\left(-\frac{u}{V}\right) \quad (u \geq 0);$$

where V is the average height to be reached in a hop. For a CRR trapped in a well with depth v , the probability of rearrangement in a hop reads

$$Q(v) = \int_v^\infty q(u)du = \exp\left(-\frac{v}{V}\right):$$

The rate of rearrangement,

$$\dot{\gamma}(v) = \nu_0 Q(v);$$

equals the number of hops (per unit time) in which a point reaches the liquid-like level,

$$\dot{\gamma}(v) = \nu_0 \exp\left(-\frac{v}{V}\right): \quad (1)$$

Denote by N_a and N_p the numbers of active and passive CRRs per unit mass, and by $p(v)$ the distribution of potential wells with various energies v . The rearrangement process is described by the function $n(t; v)$ that equals the number (per unit mass) of active CRRs trapped in wells with energy v which have last been rearranged before instant $t - \tau_0$. The quantity $n(t; v)$ is the current number of active CRRs (per unit mass) with energy v ,

$$n(t; v) = N_a p(v): \quad (2)$$

The quantity

$$\frac{\partial n}{\partial t}(t; v)dt$$

equals the number (per unit mass) of active CRRs with energy v that have last been rearranged during the interval $[t; t + dt]$ and, afterwards, have not been rearranged within the interval $[t; t]$. The number of active CRRs (per unit mass) with energy v that were rearranged (for the first time) within the interval $[t; t + dt]$ is given by

$$\frac{\partial n}{\partial t}(t; 0; v)dt;$$

and the number (per unit mass) of active CRRs with energy v that have been rearranged within the interval $[t; t + dt]$, and, afterwards, were rearranged during the interval $[t; t + dt]$ reads

$$\frac{\partial^2 n}{\partial t^2}(t; v)dt^2 :$$

The rate of rearrangement, λ , is defined as the ratio of the number of active CRRs rearranged per unit time to the total number of active CRRs,

$$\begin{aligned} \frac{\partial n}{\partial t}(t; 0; v) &= \lambda(v)n(t; 0; v); \\ \frac{\partial^2 n}{\partial t^2}(t; v) &= \lambda(v)\frac{\partial n}{\partial t}(t; v): \end{aligned}$$

The solutions of these equations with initial condition (2) read

$$\begin{aligned} n(t; 0; v) &= N_a p(v) \exp(-\lambda(v)t); \\ \frac{\partial n}{\partial t}(t; v) &= N_a p(v) \lambda(v) \exp(-\lambda(v)t) : \end{aligned} \quad (3)$$

3 Constitutive equations

At uniaxial deformation with small strains, a CRR is modelled as a linear elastic medium with the strain energy

$$w = \frac{1}{2} e^2;$$

where κ is an average rigidity per CRR and e is the strain from the reference state of a relaxing unit to its deformed state. We assume that CRRs are connected by links that transmit the macro-strain in an ensemble, ϵ , to individual regions. This means that for a passive CRR (that is not rearranged within the experimental time-scale), as well as for an active CRR that has not been rearranged before time t , the strain e coincides with the macro-strain $\epsilon(t)$. For a CRR that has last been rearranged at time $t_2 \in [0; t]$, the reference state coincides with the state of the ensemble at the instant of rearrangement, which implies that the strain, e , equals the difference between the current macro-strain, $\epsilon(t)$, and the macro-strain, $\epsilon(t_2)$, at the instant of rearrangement, t_2 .

To calculate the strain energy density per unit mass, $W(t)$, we multiply the mechanical energy per CRR by the number of relaxing units and sum the mechanical energies of

passive CRRs and active CRRs rearranged at various instants $t \in [0; t]$. Neglecting the energy of interaction between relaxing units, we find that

$$W(t) = \frac{1}{2} N_p + \int_0^{Z_1} n(t; 0; v) dv + \int_0^{Z_1} dv \int_0^{Z_t} \frac{\partial n}{\partial t}(t; v) dt + \int_0^{Z_1} \int_0^{Z_t} \frac{\partial^2 n}{\partial t^2}(t; v) dt dv; \quad (4)$$

Differentiation of Eq. (4) with respect to time results in

$$\frac{dW}{dt}(t) = A(t) \frac{d}{dt}(t) + Y(t); \quad (5)$$

$$A(t) = N(t) \int_0^{Z_t} \left(\int_0^{Z_1} (v) \exp(v(t)) p(v) dv \right) dv; \quad (6)$$

$$Y(t) = \frac{1}{2} \int_0^{Z_1} (v) dv n(t; 0; v)^2(t) + \int_0^{Z_t} \frac{\partial n}{\partial t}(t; v) dt \int_0^{Z_1} (v)^2 dv; \quad (7)$$

where $N = N_a + N_p$ and $\rho = N_a / N$. For isothermal uniaxial deformation, the Clausius-Duhem inequality reads

$$\dot{\rho} = \frac{dW}{dt} + \frac{d}{dt} \rho \geq 0;$$

where ρ is mass density, σ is stress, and $\dot{\rho}$ is internal dissipation per unit mass. Substitution of Eq. (5) into this equation yields

$$\dot{\rho} = \frac{1}{\rho} \left(A \right) \frac{d}{dt} + Y \geq 0;$$

It follows from Eq. (7) that $Y(t)$ is non-negative. This implies that the dissipation inequality is satisfied, provided that the first term on the right-hand side vanishes. Equating the expression in brackets to zero and using Eq. (6), we arrive at the constitutive equation

$$\sigma(t) = G(t) \int_0^{Z_t} \left(\int_0^{Z_1} (v) \exp(v(t)) p(v) dv \right) dv; \quad (8)$$

where $G = \rho N$ is an elastic modulus.

4 Dynamic mechanical tests

For an oscillatory test with an amplitude ϵ_0 and a frequency ω , the strain reads

$$\epsilon(t) = \epsilon_0 \exp(i\omega t);$$

where $i = \sqrt{-1}$. Substituting this expression into Eq. (8) and using Eq. (1), we find the storage, $G'(\omega)$, and loss, $G''(\omega)$, moduli

$$G'(\omega) = G_1 \int_0^{Z_1} \frac{\epsilon_0^2 \exp(-2z)}{\epsilon_0^2 \exp(-2z) + \omega^2} P(z) dz; \\ G''(\omega) = G_0 \omega \int_0^{Z_1} \frac{\epsilon_0 \exp(-z)}{\epsilon_0^2 \exp(-2z) + \omega^2} P(z) dz; \quad (9)$$

where

$$z = \frac{V}{V_0}; \quad V_0 = V; \quad P(z) = p(Vz):$$

Restrictions on the upper boundary of a frequency window in conventional mechanical tests (the maximal frequency does not exceed 1 kHz) imply that the shape of the distribution function $P(z)$ at small z cannot be uniquely determined by fitting observations. To avoid ambiguities, we set

$$P(z) = K_1 \delta(z) + K_2 P_0(z); \quad (10)$$

where $\delta(z)$ is the Dirac delta-function, K_m ($m = 1, 2$) are non-negative constants such that $K_1 + K_2 = 1$, and $P_0(z)$ is the distribution function corresponding to the range of frequencies "visible" in the frequency window. With reference to [8], the following expression is adopted for the function $P_0(z)$:

$$P_0(z) = \frac{1}{6Z} \frac{z^3}{Z^3} \exp\left(-\frac{z}{Z}\right); \quad (11)$$

where

$$Z = \frac{hzi}{4}$$

and hzi is the average activation energy per CRR. Substitution of Eq. (10) into Eq. (9) results in

$$\begin{aligned} G^0(\omega) &= G \left[k_1 \frac{\omega^2}{\omega_0^2 + \omega^2} + k_3 + k_2 \omega_0^2 \int_0^{\omega/\omega_0} \frac{P_0(z) dz}{\exp(-2z) + \omega_0^2} \right]; \\ G''(\omega) &= G \left[k_1 \frac{\omega}{\omega_0^2 + \omega^2} + k_2 \omega_0^2 \int_0^{\omega/\omega_0} \frac{\exp(-z) P_0(z) dz}{\exp(-2z) + \omega_0^2} \right]; \end{aligned} \quad (12)$$

where $k_1 = \omega_0 K_1$, $k_2 = \omega_0 K_2$, and $k_3 = 1 - \omega_0$. The coefficient k_1 is the concentration of CRRs whose rates of rearrangement substantially exceeds the maximal frequency of oscillations ("viscous" units), k_2 is the concentration of CRRs whose rates of rearrangement belong to the frequency window of dynamic tests ("viscoelastic" units), and k_3 is the fraction of CRRs whose rates of rearrangement is noticeably less than the minimal frequency of vibrations ("elastic" units).

Equations (11) and (12) are determined by 5 material constants:

1. the elastic modulus G ,
2. the attempt rate ω_0 ,
3. the average activation energy per CRR hzi ,
4. the fraction of "viscous" CRRs k_1 ,
5. the fraction of "elastic" CRRs k_3 .

These parameters are found by fitting experimental data for a multicomponent silicate glass.

5 Validation of the model

We study the mechanical response of a rock wool glass with the chemical composition (wt.-%) 41.9 SiO₂, 17.0 Al₂O₃, 18.3 CaO, 12.5 MgO, 0.3 K₂O, 1.4 TiO₂, 5.7 FeO, 2.0 Na₂O. Torsional dynamic tests were performed by N.S. Bagdasarov (University of Frankfurt, Germany) at temperatures ranged from 500 to 760 °C (this interval includes the glass transition point T_g = 678 °C). For a description of specimens and the experimental procedure, see [9]. The effect of temperature on the viscoelastic behavior of the glass is demonstrated by Figure 1, where the loss tangent (at the frequency f = 1 Hz) is plotted versus temperature. To approximate observations, we present Eqs. (12) in the form

$$\begin{aligned} G^0(\omega) &= \omega^2 \frac{C_1}{\omega_0^2 + \omega^2} + \frac{C_3}{\omega^2} + C_2 \int_0^{\omega_1} \frac{P_0(z) dz}{\omega_0^2 \exp(-2z) + \omega^2}; \\ G''(\omega) &= \omega \frac{C_1 \omega_0}{\omega_0^2 + \omega^2} + C_2 \int_0^{\omega_1} \frac{\omega_0 \exp(-z) P_0(z) dz}{\omega_0^2 \exp(-2z) + \omega^2}; \end{aligned} \quad (13)$$

where C_m = Gk_m (m = 1;2;3).

To find ω₀, Z and C_m at a given temperature, T, we fix some intervals [0; ω_{max}] and [0; Z_{max}], where the "best-fit" parameters ω₀ and Z are assumed to be located, and divide these intervals into J subintervals by the points ω^(j) = j ω_{max}/J and Z^(k) = k Z_{max}/J (j,k = 1;...;J) with ω_{max} = J and Z_{max} = J. For any pair, ω^(j); Z^(k), the constants C_m = C_m(j;k) are found by the least-squares technique from the condition of minimum of the function

$$M(j;k) = \sum_{\omega_1}^{\omega_h} G_{\text{exp}}^0(\omega_1) - G_{\text{num}}^0(\omega_1)^2 + G_{\text{exp}}''(\omega_1) - G_{\text{num}}''(\omega_1)^2;$$

where G_{exp}⁰ and G_{exp}^{''} are the storage and loss moduli measured in a test, the quantities G_{num}⁰ and G_{num}^{''} are given by Eqs. (13), and the sum is calculated over all frequencies ω₁. The "best-fit" parameters ω₀ and Z minimize the function M on the set ω^(j); Z^(k) (j,k = 1;...;J). After the constants C_m are determined, the elastic modulus, G, and the constants k_m are calculated by the formulas G = C₁ + C₂ + C₃, k_m = C_m/G. The elastic modulus is plotted versus temperature T in Figure 14, and the constants, k_m, are depicted in Figures 15 and 16. The experimental data are approximated by the linear equations

$$G = G_0 - G_1 T; \quad k_m = k_{m0} + k_{m1} T; \quad (14)$$

where G_j and k_{m,j} (j = 0;1) are found by the least-squares technique. The quantities hzi = 4Z and ω₀ are plotted versus temperature in Figure 17 together with their mean values hzi = 1.35 and ω₀ = 0.14 s⁻¹.

6 Discussion

Figure 14 shows that G is independent of T in the sub-T_g region, and it decreases with T above T_g. This conclusion is in accord with the conventional assertion that the elastic modulus falls down when the temperature reaches the glass transition point. A decrease

in G with temperature is quite noticeable (the modulus is reduced by 32 %), but it is substantially less than that in polymeric glasses (where elastic moduli drop by several orders of magnitude as temperature passes through the glass transition point).

Figures 15 and 16 reveal that the concentration of "viscous" CRR increases with temperature both below and above the glass transition point, whereas the fractions of "elastic" and viscoelastic relaxing units remain practically constant below T_g . The latter means that only a portion of passive CRRs with negligible potential energies become activated in the sub- T_g region. Above the glass transition point, k_1 and k_2 substantially increase with temperature, while k_3 pronounsly decreases. This reflects transformation of passive relaxing units into active "viscous" and "viscoelastic" CRRs induced by thermal fluctuations.

Figure 17 demonstrates that the attempt rate, ν_0 , and the average activation energy of CRRs, $\langle E_a \rangle$, are independent of temperature. The fact that the energy landscape of a glass is not affected by temperature appears to be rather natural [10]. To explain why ν_0 remains temperature-independent, we refer to the Narayanaswamy theory [11]. According to it, rearrangement of CRRs is governed by some effective temperature, T_e ,

$$\frac{1}{T_e} = \frac{1}{T} + \frac{1}{T_f}; \quad (15)$$

where T_f is the fictive temperature (that characterizes changes in the internal structure of a glass), and $\beta \in [0;1]$ is a material constant. With an increase in temperature, the first term on the right-hand side of Eq. (15) decreases. This decrease is, however, compensated by an increase in the other term: given a duration of a dynamic test, structural recovery in a glass occurs more intensively at a higher temperature, which implies that a drop in the fictive temperature (that approaches the current temperature for an equilibrated glass) is more pronounced compared to that at a low temperature.

It is worth to compare Eq. (8) with other micro-mechanical concepts in viscoelasticity of glasses. The ADWP (asymmetric double-well potential) model [12] does not account for the presence of "viscous" CRRs that play the key role in the time-dependent response (Figure 15). The SGR (soft glassy rheology) model [13] presumes strain-induced transformations of the energy landscape that are not observed in experiments (Figure 17).

7 Concluding remarks

Constitutive equations have been developed for the viscoelastic behavior of a silicate glass at isothermal uniaxial loading with small strains. A glass is treated as an ensemble of independent units, where relaxation of stresses is driven by cooperative rearrangement of clusters of atoms. The rearrangement process is thought of as a series of hops of CRRs (trapped at the bottom levels of their potential wells on the energy landscape) to higher energy levels. The ensemble is split into three groups of relaxing units: "elastic" CRRs, whose rate of rearrangement is substantially less than the minimal frequency, "viscous" CRRs whose rate of rearrangement noticeably exceeds the maximal frequency, and "viscoelastic" CRRs, whose rate of rearrangement is comparable with frequencies of dynamic tests. Explicit expressions have been derived for the storage and loss moduli.

These formulas are determined by 5 adjustable parameters that are found by matching experimental data for a multicomponent silicate glass at temperatures in the vicinity of the glass transition point. It is demonstrated that the attempt rate for hops and the distribution of potential wells with various depths are independent of temperature, whereas the instantaneous elastic modulus and the concentrations of "elastic", "viscous" and "viscoelastic" relaxing units are strongly affected by temperature. With an increase in T , the fraction of "elastic" units decreases, and the concentrations of "viscous" and "viscoelastic" units increase, which is ascribed to thermally-induced activation of passive CRRs.

References

- [1] Fanderlik, I. *Silica Glass and its Application*, Elsevier, Amsterdam (1991).
- [2] Mysen, B.O. *Structure and Properties of Silicate Melts*, Elsevier, Amsterdam (1988).
- [3] van der Brink, J.P.J. *Non-Cryst. Solids*, 196, 210 (1996).
- [4] Du renne, L., Gy, R., Burlet, H., Piques, R. *Non-Cryst. Solids*, 215, 208 (1997).
- [5] Pelletier, J.M., Perez, J., Du renne, L. *Acta Mater.*, 48, 1397 (2000).
- [6] Goldstein, M.J. *Chem. Phys.*, 51, 3728 (1969).
- [7] Bouchaud, J.P.J. *Phys. I (France)*, 2, 1705 (1992).
- [8] Wiedersich, J., Surovtsev, N.V., Novikov, V.N., Rossler, E., Sokolov, A.P. *Phys. Rev. B*, 64, 064207 (2001).
- [9] Bagdasarov, N., Dorfman, A. *Tectonophys.*, 290, 27 (1998).
- [10] Wiedersich, J., Aichtchev, S.V., Rossler, E. *Phys. Rev. Lett.*, 84, 2718 (2000).
- [11] Narayanaswamy, O.S. *J. Am. Ceram. Soc.*, 52, 554 (1971).
- [12] Buchenau, U. *Phys. Rev. B*, 63, 104203 (2001).
- [13] Sollich, P. *Phys. Rev. E*, 58, 738 (1998).

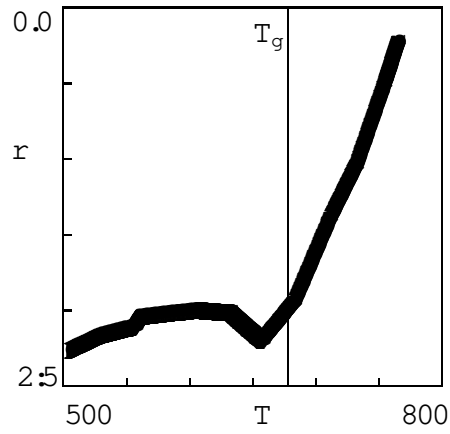


Figure 1: The loss tangent $r = \log \tan$ versus temperature T °C. Circles: treatment of observations. Solid line: approximation of the experimental data by a piecewise linear function. The vertical line indicates the glass transition temperature

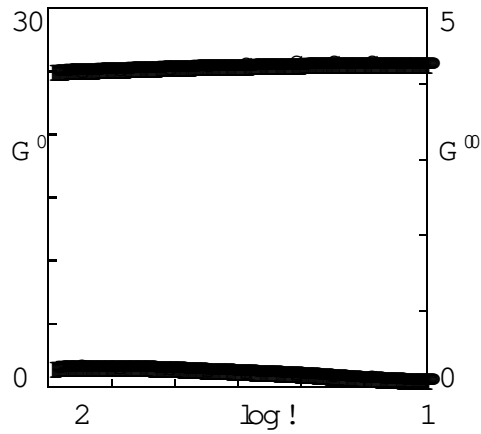


Figure 2: The storage modulus G' GPa (un filled circles) and the loss modulus G'' GPa (filled circles) versus frequency ω rad/s. Symbols: experimental data ($T = 500 \pm 10$ °C). Solid lines: numerical simulation

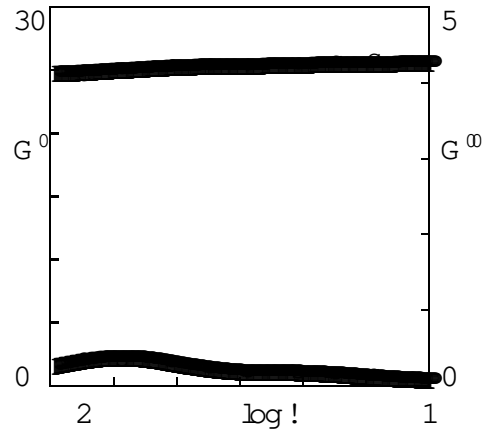


Figure 3: The storage modulus G' GPa (un filled circles) and the loss modulus G'' GPa (filled circles) versus frequency ω rad/s. Symbols: experimental data ($T = 526.5^\circ\text{C}$). Solid lines: numerical simulation

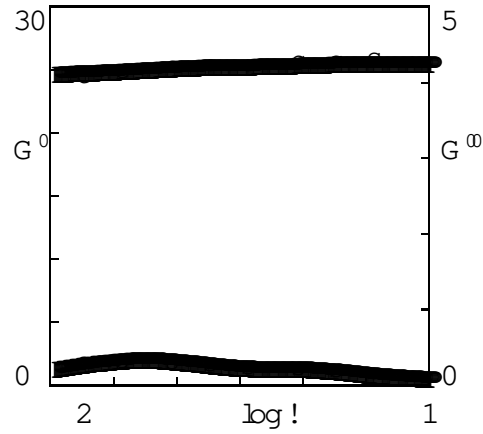


Figure 4: The storage modulus G' GPa (un filled circles) and the loss modulus G'' GPa (filled circles) versus frequency ω rad/s. Symbols: experimental data ($T = 552.0^\circ\text{C}$). Solid lines: numerical simulation

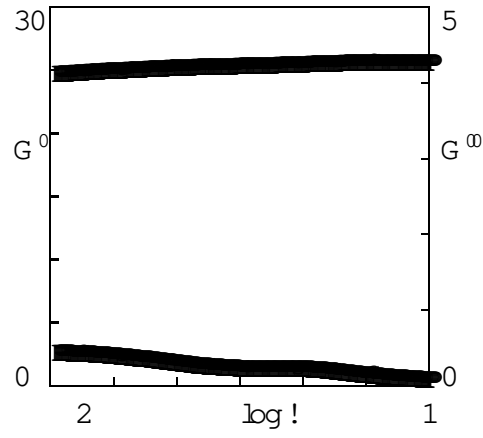


Figure 5: The storage modulus G' GPa (un filled circles) and the loss modulus G'' GPa (filled circles) versus frequency ω rad/s. Symbols: experimental data ($T = 577.0$ C). Solid lines: numerical simulation

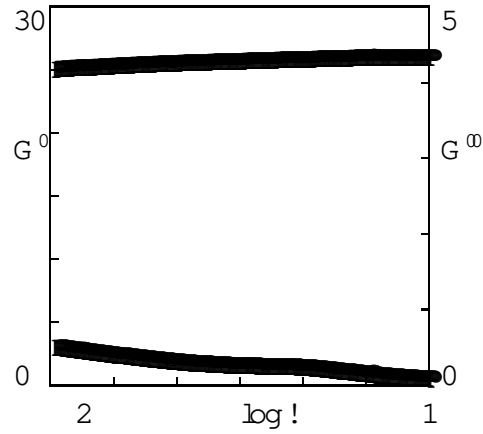


Figure 6: The storage modulus G' GPa (un filled circles) and the loss modulus G'' GPa (filled circles) versus frequency ω rad/s. Symbols: experimental data ($T = 601.5$ C). Solid lines: numerical simulation

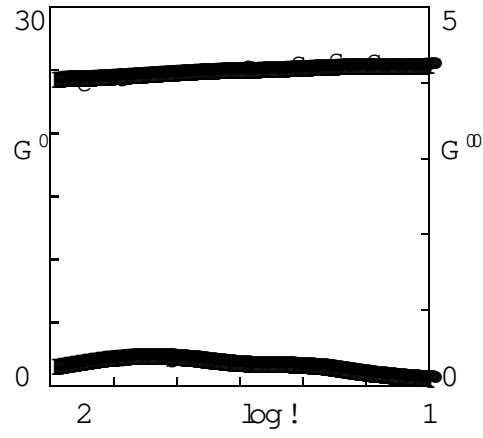


Figure 7: The storage modulus G' GPa (un filled circles) and the loss modulus G'' GPa (filled circles) versus frequency ω rad/s. Symbols: experimental data ($T = 627.5$ C). Solid lines: numerical simulation

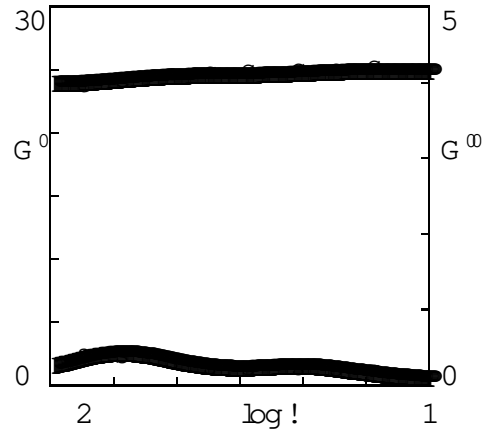


Figure 8: The storage modulus G' GPa (un filled circles) and the loss modulus G'' GPa (filled circles) versus frequency ω rad/s. Symbols: experimental data ($T = 653.0$ C). Solid lines: numerical simulation

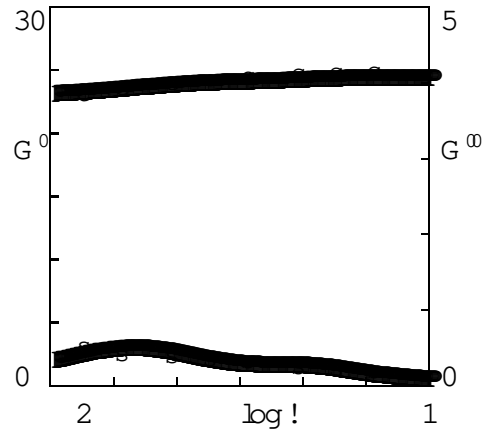


Figure 9: The storage modulus G' GPa (un filled circles) and the loss modulus G'' GPa (filled circles) versus frequency ω rad/s. Symbols: experimental data ($T = 678.0$ K). Solid lines: numerical simulation

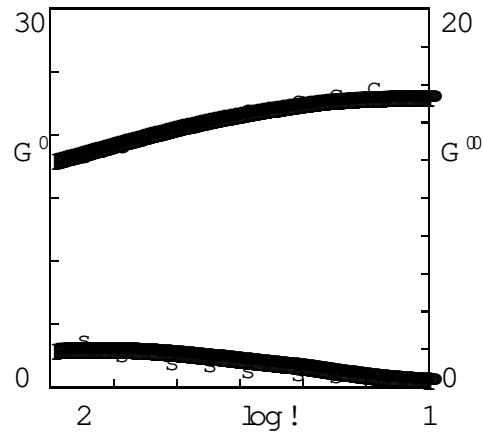


Figure 10: The storage modulus G' GPa (un filled circles) and the loss modulus G'' GPa (filled circles) versus frequency ω rad/s. Symbols: experimental data ($T = 706.5$ K). Solid lines: numerical simulation

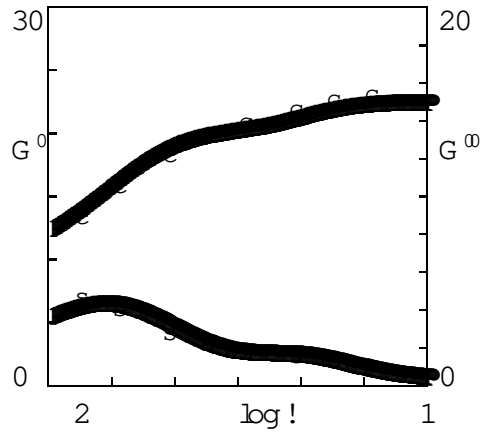


Figure 11: The storage modulus G' GPa (un filled circles) and the loss modulus G'' GPa (filled circles) versus frequency ω rad/s. Symbols: experimental data ($T = 727.0$ C). Solid lines: numerical simulation

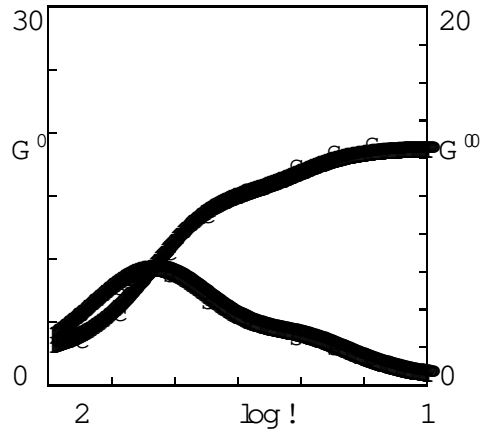


Figure 12: The storage modulus G' GPa (un filled circles) and the loss modulus G'' GPa (filled circles) versus frequency ω rad/s. Symbols: experimental data ($T = 749.5$ C). Solid lines: numerical simulation

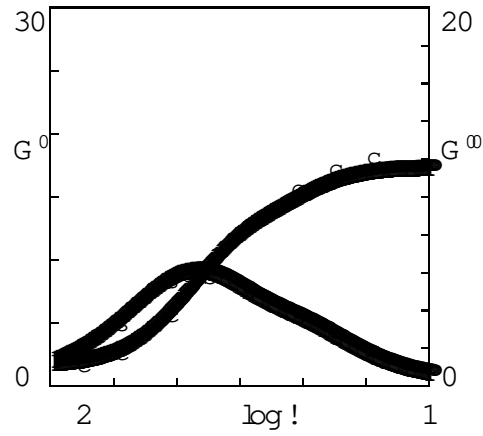


Figure 13: The storage modulus G' GPa (un filled circles) and the loss modulus G'' GPa (filled circles) versus frequency ω rad/s. Symbols: experimental data ($T = 760.0$ C). Solid lines: numerical simulation

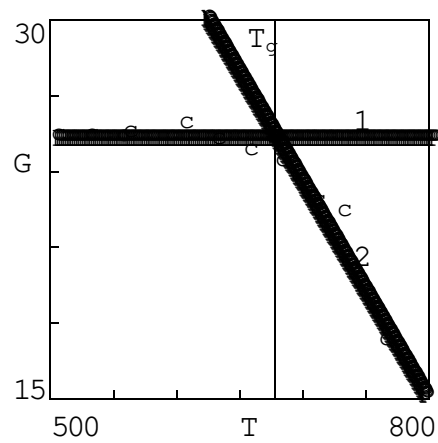


Figure 14: The elastic modulus G GPa versus temperature T C. Circles: treatment of observations. Solid lines: approximation of the experimental data by Eq. (14). Curve 1: $G_0 = 25.23, G_1 = 0.0$; curve 2: $G_0 = 83.48, G_1 = 8.63 \cdot 10^2$

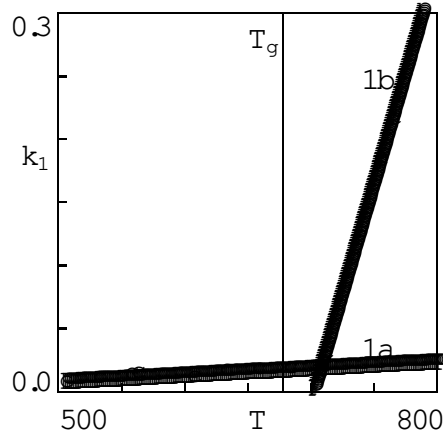


Figure 15: The dimensionless parameter k_1 versus temperature T °C. Circles: treatment of observations. Solid lines: approximation of the experimental data by Eq. (14). Curve 1a: $k_{10} = 2.09 \cdot 10^2$, $k_{11} = 5.31 \cdot 10^4$; curve 1b: $k_{10} = 2.43$, $k_{11} = 3.48 \cdot 10^3$

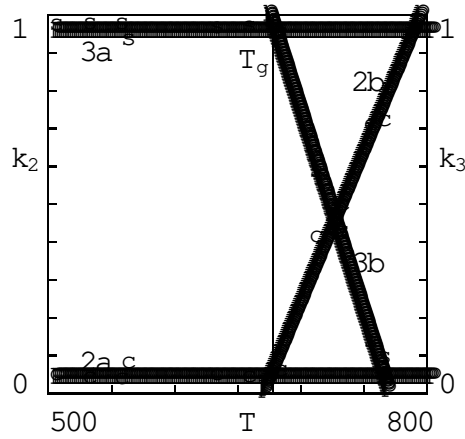


Figure 16: The dimensionless parameters k_2 (unfilled circles) and k_3 (filled circles) versus temperature T °C. Symbols: treatment of observations. Solid lines: approximation of the experimental data by Eq. (14). Curve 2a: $k_{20} = 3.80 \cdot 10^2$, $k_{21} = 0.0$; curve 2b: $k_{20} = 5.34$, $k_{21} = 8.02 \cdot 10^3$; curve 3a: $k_{30} = 0.95$, $k_{31} = 0.0$; curve 3b: $k_{30} = 8.10$, $k_{31} = 1.06 \cdot 10^2$

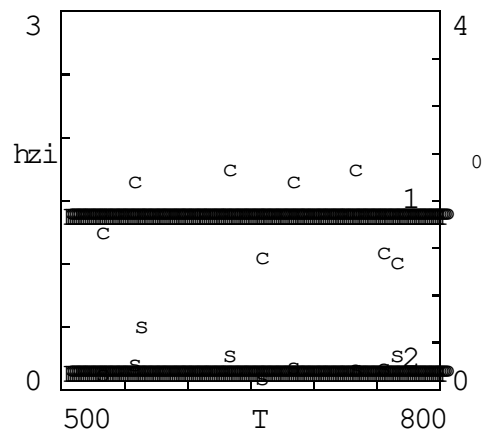


Figure 17: The average activation energy per CRR hzi (un filled circles) and the attempt rate s^{-1} (filled circles) versus temperature T $^{\circ}C$. Symbols: treatment of observations. Curves 1 and 2: the mean values